



FORTE 2.0: a fast, parallel and flexible coupled climate model

Adam T. Blaker¹, Manoj Joshi², Bablu Sinha¹, David P. Stevens³, Robin S. Smith⁴, and Joël J.-M. Hirschi¹

¹National Oceanography Centre, European Way, Southampton, UK

²Climatic Research Unit, School of Environmental Sciences, University of East Anglia, Norwich, UK

³Centre for Ocean and Atmospheric Sciences, School of Mathematics, University of East Anglia, Norwich, UK

⁴NCAS, Dept. of Meteorology, University of Reading, Reading, UK

Correspondence: Adam T. Blaker (atb299@noc.ac.uk)

Received: 10 February 2020 – Discussion started: 5 March 2020

Revised: 18 November 2020 – Accepted: 30 November 2020 – Published: 19 January 2021

Abstract. FORTE 2.0 is an intermediate-resolution coupled atmosphere–ocean general circulation model (AOGCM) consisting of the Intermediate General Circulation Model 4 (IGCM4), a T42 spectral atmosphere with 35σ layers, coupled to Modular Ocean Model – Array (MOMA), a $2^\circ \times 2^\circ$ ocean with 15 z -layer depth levels. Sea ice is represented by a simple flux barrier. Both the atmosphere and ocean components are coded in Fortran. It is capable of producing a stable climate for long integrations without the need for flux adjustments. One flexibility afforded by the IGCM4 atmosphere is the ability to configure the atmosphere with either 35σ layers (troposphere and stratosphere) or 20σ layers (troposphere only). This enables experimental designs for exploring the roles of the troposphere and stratosphere, and the faster integration of the 20σ layer configuration enables longer duration studies on modest hardware. A description of FORTE 2.0 is given, followed by the analysis of two 2000-year control integrations, one using the 35σ configuration of IGCM4 and one using the 20σ configuration.

1 Introduction

Numerical models of the coupled (atmosphere–ocean) climate system are important tools for studying the Earth’s climate. They provide insight into phenomena which are difficult to observe directly, such as the Atlantic Meridional Overturning Circulation (AMOC) or the effects of increasing atmospheric CO₂. They can also be used to test hypotheses about the global climate and the world we live in. In a climate model, it is possible to study the climate response to extreme events such as loss of ice cover (and the resulting

change in albedo). Whilst the results in terms of quantitative changes to temperature, precipitation and other climate variables should be treated with caution, it is possible to examine the processes which lead to the predicted changes.

There is a broad spectrum of coupled climate models. At one end of the spectrum are coarse-resolution simplified models designed to run millennial-scale experiments quickly and for minimal computational cost, both in terms of computing power and memory resources (e.g. GENIE, Marsh et al., 2007; CLIMBER, Montoya et al., 2005; UVic, Weaver, 2004; ECBilt, Haarsma et al., 1996). At the opposite end of the spectrum, high-resolution (< 0.1–0.5° ocean) models (e.g. those contributing to the CMIP6 HighResMIP, Haarsma et al., 2016, such as HadGEM3-GC3.1, Roberts et al., 2019, and HiGEM, Shaffrey et al., 2009). Between the two extremes are the intermediate-resolution models (e.g. HadCM3, Gordon et al., 2000; FAMOUS, Smith et al., 2008), including most of the coupled climate models contributing to CMIP3 (Meehl et al., 2007), CMIP5 (Taylor et al., 2012) and CMIP6 (Eyring et al., 2016). It is worth noting that model development does not equate solely to an increase in horizontal resolution. Inclusion of more, or better parameterised, Earth system processes can be an equally if not more important development (e.g. Sellar et al., 2019).

Sinha and Smith (2002) developed FORTE (Fast Ocean Rapid Troposphere Experiment), a fast and flexible coupled climate model, for the purposes of climate studies. FORTE’s speed and flexibility meant that the original model was an ideal educational and research tool. The flexibility of FORTE is evident in the variety of experiments in which it has been used to study ocean and/or climate phenomena. Examples include Buchan et al. (2014), in which observed sea surface

temperature (SST) anomalies from 2009 to 2010 were applied to the model SST field prior to the coupling time step, enabling the authors to examine the effect of observed SST anomalies in an otherwise free-running coupled model; in Sinha et al. (2012), the simplicity of FORTE made it easy to examine the effect of orography on the AMOC; Wilson et al. (2009) used the flexibility to examine the roles of orography and ocean dynamics on atmospheric storm tracks, performing experiments with either an interactive ocean or the static mixed layer option in the Intermediate General Circulation Model (IGCM) atmosphere; Blaker et al. (2006) added initial condition perturbations to the Southern Ocean to study fast ocean teleconnection processes; and Atkinson et al. (2009) performed similar experiments using both ocean-only and coupled configurations. Although most studies used FORTE with a T42 resolution atmosphere and 2° ocean, a version of FORTE using a T21 resolution atmosphere and 4° ocean has also been used for idealised experiments featuring Pangean and aquaplanet configurations (e.g. Smith et al., 2004, 2006). Simulations of FORTE have also been analysed in other climate studies (Hunt et al., 2013; Grist et al., 2008). However, until now, there has been no comprehensive, peer-reviewed publication describing the model itself.

A new version of the atmosphere component of FORTE was released in 2015, and a desire to perform coupled experiments once again resulted in a refresh of FORTE. To avoid confusion with earlier endeavours but at the same time make clear the ancestry of the model, we decided to refer to the refreshed model as FORTE 2.0. This paper describes the coupled model and its components and demonstrates that FORTE 2.0 produces a realistic and stable climate without the need for flux adjustments. The control integrations described are 2000-year integrations starting from rest with the Levitus (temperature, salinity) climatology (Levitus and Boyer, 1998; Levitus et al., 1998) and pre-industrial atmospheric concentrations of CO_2 . The model is forced solely by incoming solar radiation at the top of the atmosphere. The rest of this paper is organised as follows: Sect. 2 gives a description of FORTE 2.0; Sect. 3 presents the model spin-up; Sect. 4 presents the control climate; Sect. 5 discusses the main modes of climate variability in the model; Sect. 6 concludes the paper.

2 Model description

FORTE 2.0 is a global coupled atmosphere–ocean general circulation model consisting of a 2° resolution configuration of the MOMA (Modular Ocean Model – Array) (Webb, 1996) ocean model coupled to a T42 (approximately 2.8°) configuration of the IGCM4 (Joshi et al., 2015) atmosphere model. FORTE 2.0 is an updated incarnation of FORTE (Fast Ocean Rapid Troposphere Experiment) (Sinha and Smith, 2002; Smith et al., 2004), with the most significant changes being an increase in horizontal resolution of both the ocean

and atmosphere components by a factor of 2 and an update of the atmosphere code from IGCM3 (Forster et al., 2000) to IGCM4 (Joshi et al., 2015).

The ocean and atmosphere components of FORTE 2.0 are coupled once per model day using OASIS version 2.3 (Terray et al., 1999) and PVM version 3.4.6 (Parallel Virtual Machine; see <http://www.csm.ornl.gov/pvm/>, last access: 18 November 2020, Geist et al., 1994). Daily average quantities of the variables that are to be exchanged are stored in arrays, and at the end of each model day these are passed to the coupler. MOMA provides daily mean values of sea surface temperature, zonal and meridional velocities, whilst IGCM4 provides solar and non-solar heat fluxes, net freshwater flux, and zonal and meridional surface wind stress. Interpolation between the ocean and atmosphere grids is performed by the coupler using a pre-computed set of weights to ensure conservation.

Integration is relatively fast (~ 100 model years per wall-clock day on a 28-core 2.4 GHz Intel Broadwell CPU), and the model can be run on a desktop computer, making it ideal for experiments where more complex higher-resolution models are resource limited. The retention of the full primitive equations for fluid flow in both atmosphere and ocean allows more realistic simulations than possible with Earth models of intermediate complexity (EMICs). In addition, FORTE 2.0 is readily configurable, allowing experiments with realistic and idealised configurations of coastlines, orography and ocean bottom topography.

2.1 The atmosphere component

The atmosphere component of FORTE 2.0 is IGCM4 (Joshi et al., 2015), run with a T42 spectral resolution. A longitudinally regular and Gaussian in latitude grid with a grid spacing of 2.8° is used for advection and diabatic processes. The resolution is sufficient to enable stable climate integrations without the need for flux adjustments. There are two pre-configured choices for the number of vertical levels: a troposphere-only atmosphere represented by 20σ levels (L20) which extends to around 25 km altitude or a 35σ level configuration (L35) which includes the stratosphere and extends to around 65 km altitude. To avoid issues with $2\Delta z$ oscillations under certain conditions, the NIKOSRAD radiation scheme in IGCM3 (used previously in FORTE) was replaced with a modified version of the Morcrette radiation scheme (Zhong and Haigh, 1995). For further details of the IGCM4 and its performance, we refer the reader to Joshi et al. (2015) and references therein. The model is run with 96 (L35) or 72 (L20) time steps per day. Orography is derived from the US Naval 1/6th degree resolution dataset. IGCM4 is Message Passing Interface (MPI) parallelised, and at this resolution integration on 16–32 cores achieves the best performance.

Atmospheric convection is dealt with via a Betts–Miller scheme (Betts and Miller, 1993). Low, medium and high layer clouds and convective cloud amounts are represented

based on a critical relative humidity criterion (see the Appendix of Forster et al., 2000). The formula which determines low-level cloud amount has an additional factor of 50 % compared to that used by Forster et al. (2000) to correct a cold bias within the tropical ocean which led to unrealistic circulation in the Pacific. In addition to variation with solar zenith angle (and hence latitude), sea surface albedo is increased away from polar regions to compensate for the absence of aerosols which would otherwise scatter incoming solar radiation. Land grid boxes are assigned a vegetation index, one of 24 pre-defined vegetation types, which determine the albedo and roughness length.

Coupling to the dynamic ocean model requires some changes to the surface boundary layer. In order to conserve water, it is necessary to account for soil moisture and implement river runoff. Soil moisture for each land grid box is represented as a bucket, or reservoir, 0.5 m in depth. Excess water, i.e. when the volume of water is greater than the volume of the bucket, is accumulated and added to the ocean as runoff at each coupling time step. The land surface is divided into catchment basins, and the accumulated runoff is distributed on a list of predetermined atmospheric grid cells that lie over the ocean and represent river mouths. The catchment areas and river discharge points are derived from Weaver et al. (1998), as explained in Sinha and Smith (2002). Runoff accumulated over Antarctica is distributed uniformly over the ocean south of 55° S, as a simplistic representation of iceberg calving and melting. Additionally, land snow cover is capped at a maximum thickness of 4 m. Excess snow over Antarctica and the Arctic region is treated separately as an additional runoff term that represents iceberg melting and calving. As with the soil moisture, runoff from excess snow over Antarctica is distributed uniformly over the ocean south of 55° S. Excess snowmelt over the Arctic is handled similarly, with a uniform distribution over the ocean north of 66° N.

A coastal tiling routine is implemented in order to handle the differences between the atmosphere and ocean grids. Grid cells in the ocean are either ocean or land, whilst atmospheric grid cells can be ocean, land or partial (i.e. they extend over both ocean and land cells on the ocean grid). Atmospheric grid cells that wholly overlie ocean are updated using the normal IGCM4 boundary layer scheme and the SST from the ocean model that is exchanged through the coupler. Similarly, cells that wholly overlie land are updated using the IGCM4 land surface scheme. For partial atmosphere grid cells, two sets of boundary layer variables (e.g. latent heat flux) exist. One set is updated like any other land point using the IGCM4 boundary layer scheme, and the other set is updated like any other ocean point. The atmosphere then sees the weighted average of the heat fluxes over the land and sea. Care is taken to ensure that atmospheric moisture is conserved and that precipitation is also apportioned correctly between the land surface scheme and the ocean fraction of the atmosphere cell.

To improve the representation of the effects of sea surface roughness on momentum exchange, a wind-dependent drag coefficient, C_d , is implemented, such that $C_d = C_d^0 + 5.6e^{-5} \cdot \min(U_{10}, 40)$, where U_{10} is the 10 m wind speed (Wu, 1980). This gives a maximum $C_d = 0.003$ at a wind speed of 40 m s^{-1} without ice cover. C_d^0 is the drag coefficient over ocean cells, calculated using a globally uniform value for surface roughness over the open ocean.

At present, FORTE 2.0 does not include dynamic sea-ice representation. Instead, sea ice is represented by a barrier to heat fluxes between the ocean and atmosphere components, which is imposed when the sea surface temperature reaches 271 K, and surface albedo is increased to 0.6 to represent ice cover. The albedo continues to linearly increase, reaching 0.8 at 261 K as a means to represent the albedo effects of snow on ice. Once the albedo reaches 0.8, it will not reduce until the temperature rises above freezing point and the flux barrier deactivates. There is no advection of sea ice, and salinity and runoff fluxes remain unaffected. SST under ice is relaxed toward the freezing point of seawater (-1.8°C) on a 10 d timescale.

2.2 The ocean component

The ocean component of FORTE 2.0 is MOMA (Webb, 1996), a version of the Geophysical Fluid Dynamics Laboratory (GFDL) MOM (Modular Ocean Model) (Pacanowski et al., 1990) coded to work more efficiently on array processors, which solves the primitive equations discretised using finite differences on an Arakawa B grid (Arakawa, 1966). It has a linear free surface (Killworth et al., 1991) and uses “full cell” ocean bathymetry. In the configuration used for this integration, the ocean horizontal resolution is $2^\circ \times 2^\circ$, with 15 z -layer levels, increasing in thickness with depth from 30 m at the surface to 800 m at the bottom. A polar island, comprising the top row of grid cells (88–90° N), is required in the Arctic to prevent numerical instability due to convergence of lines of longitude. There are 64 baroclinic time steps per day (22.5 min time steps) implemented using the modified split QUICK (MSQ) advection scheme (Webb et al., 1998). The version of MOMA used in FORTE 2.0 uses OpenMP shared-memory parallelisation, and running it on four to six cores is typically sufficient to match the IGCM4 performance.

Bathymetry is derived from the ETOPO5 (1988) $1/12^\circ$ resolution dataset, and interpolated onto the model resolution. Due to the horizontal resolution, in order to encourage dense water formation and flow between the Nordic Seas and North Atlantic, bathymetry is manually excavated in a manner similar to HadCM3 (Gordon et al., 2000). The Bering, Gibraltar and Kattegat/Skagerrak straits are represented by a single grid box which, due to the Arakawa B grid, means that there is no advection through them, but diffusion of potential temperature (T) and salinity (S) does occur.

Ocean isopycnal mixing is represented in MOMA through the isoneutral mixing scheme of Griffies et al. (1998). The

Table 1. Mixing parameters in MOMA.

Parameter	Value ($\text{m}^2 \text{s}^{-1}$)
Horizontal viscosity	4.0×10^3
Isopycnal tracer diffusivity	2.5×10^3
Isopycnal thickness diffusivity	2.0×10^3
Steep slope horizontal diffusivity	1.5×10^3
Vertical viscosity coefficient	1.0×10^{-3}
Bottom drag coefficient	0.001
Max. slope of isopycnals	0.002

eddy-stirring process of Gent and McWilliams (1990) is introduced as a skew flux (Griffies, 1998). Where isopycnal slopes become large, exponential tapering scales isoneutral diffusivities to zero as the slope increases (Danabasoglu and McWilliams, 1995). The isopycnal mixing parameters used for the control simulation described in Sect. 3 are shown in Table 1.

To ameliorate some of the shortcomings identified in earlier FORTE simulations, some additional changes have been made to MOMA. Firstly, the background vertical diffusion, κ , is set to be stability dependent (Gargett, 1984), albeit with the surface to sea floor potential temperature gradient as a simple proxy for stability, such that

$$\kappa_s = (0.3 + 1.7e^{-(0.15[\max(T_s, T_b) - T_b])^2}) \times 10^{-4} \text{ m}^2 \text{ s}^{-1},$$

$$\kappa = \kappa_s + (2 \times 10^{-4} - \kappa_s)z/H \text{ m}^2 \text{ s}^{-1},$$

where T_s is the surface potential temperature, T_b is the bottom potential temperature, z is depth, and H is the local total depth of the ocean. Thus, the vertical diffusivity takes a maximum value of $2 \times 10^{-4} \text{ m}^2 \text{ s}^{-1}$ at the sea floor and at high latitudes, with lower values, approaching $3 \times 10^{-5} \text{ m}^2 \text{ s}^{-1}$ in the upper ocean at low latitudes.

Secondly, starting from 5°N/S the horizontal diffusion in the surface layer increases towards the Equator from its default value to 20 times this value at the Equator to counteract equatorial upwelling and, in a simple way, parameterise the eddy heat convergence associated with tropical instability waves which was highlighted by Shaffrey et al. (2009).

3 Spinup of the control integration

To evaluate the performance of FORTE2.0, we ran a pair of control integrations with pre-industrial CO_2 concentration using both the 35σ layer and 20σ layer atmosphere configurations. In each simulation, FORTE 2.0 starts from rest with identical initial ocean temperature and salinity fields from Levitus and Boyer (1998) and Levitus et al. (1998) interpolated onto the ocean model grid. Figure 1 shows area and volume integrated quantities of the surface heat and freshwater fluxes, and ocean temperature and salinity from each of the

two integrations. The surface heat flux into the ocean is initially positive (up to 1.5 W m^{-2}) but the imbalance reduces to less than 0.5 W m^{-2} after a few decades and then stabilises and remains within $\pm 0.2 \text{ W m}^{-2}$ throughout the remainder of the integration (Fig. 1a). The time average water budget closes to within -0.2 mm yr^{-1} , after an initial adjustment in the first year of the integration (Fig. 1b). The global average SST settles within 100 years to values around 19.1°C for the L35 configuration and 19.0°C for the L20 configuration (Fig. 1c). Sea surface salinity (SSS) in both configurations adjusts more slowly, with L35 maintaining a value of around 35.15 PSU after 1000 years of integration and L20 approaching 35.23 PSU towards the end of the 2000-year simulation (Fig. 1d). The mean SST is 0.9°C warmer than the initial state provided by Levitus and Boyer (1998) (18.2°C). The volume average ocean potential temperature warms by 0.3°C for L35 and 0.2°C for L20 over the first 500 years and then cools more steadily, at a rate of approximately 0.005°C per century for L35. After 2000 years, the volume average temperature in the L20 configurations is close to the initial value. Salinity shows a gradual trend of 0.000125 PSU per century after an initial adjustment in L35, which is a reflection of the small imbalance in the freshwater fluxes. The trend in the L20 configuration is around 30 % stronger.

Global averaged time series of temperature and salinity as functions of latitude and depth are presented in Fig. 2. The time–latitude plots show an initial strong warming of the Southern Ocean that is not density compensated by an increase in salinity at the same latitudes. The onset of this warming occurs quickly and then remains stable for the remainder of the 2000-year integration. A minimal bias develops in the tropical and equatorial regions. In the Northern Hemisphere higher latitudes, there is a strong cooling that (partly) coincides with a freshening. The differences in time–latitude evolution of the SST and SSS for the L20 configuration are shown in Fig. 2c and d. High-latitude SST is slightly cooler in L20 compared with L35, except for a narrow band around $55\text{--}65^\circ \text{N}$ where a warming of a few tenths of a degree occurs. Surface salinity is marginally higher and to a large extent latitudinally uniform in L20. The difference in SSS is slightly more pronounced at the same latitude range as the narrow band of warming seen in the SSS. Analysis of the spatial SST and SSS biases presented later in this paper shows that these anomalies are located in the Nordic Seas. This pattern develops over the first 500 years of the simulation and then remains stable for the rest of the integration. The SST bias is within the range of that found in the CMIP5 ensemble (Flato et al., 2013).

The time–depth series of potential temperature (Fig. 2e) compares reasonably with those of other, higher-resolution, models such as HadCM3, HadGEM1 and CHIME (Fig. 7 in Johns et al., 2006; Fig. 3 in Megann et al., 2010). FORTE 2.0 warms above 1500 m, with the maximum difference from observed values reaching $+1.6^\circ \text{C}$ between 400 and 500 m depth. At depths below 4000 m, the ocean cools initially, with

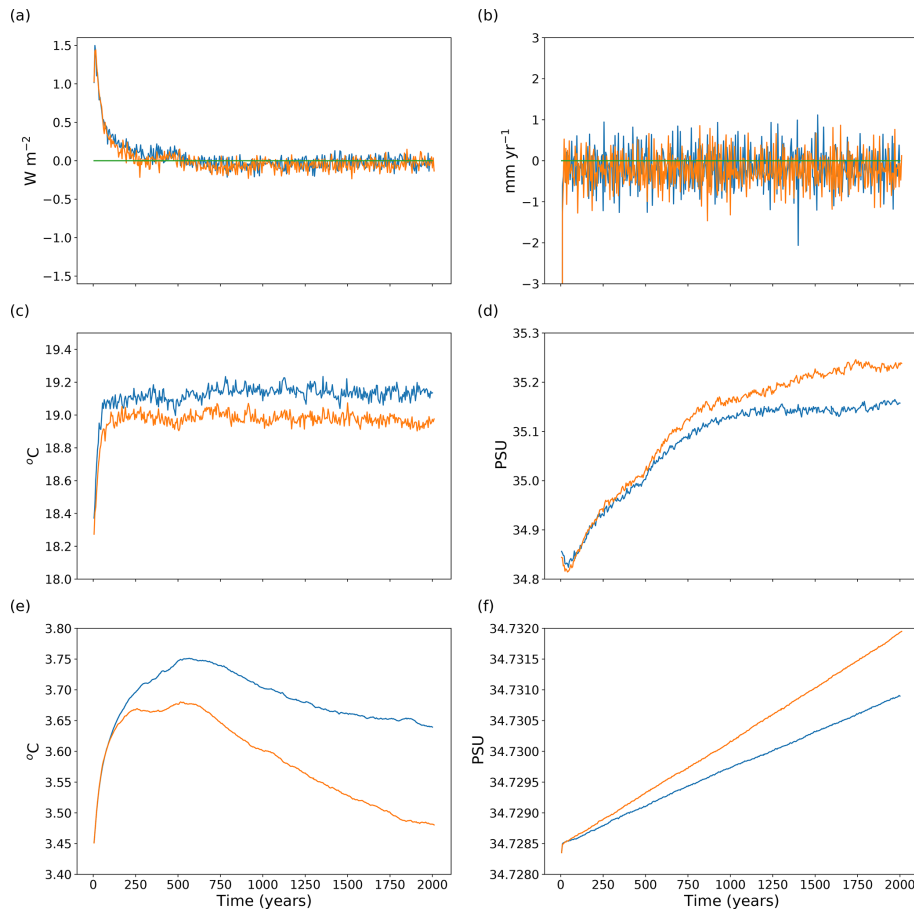


Figure 1. Time series of global mean (a) surface heat flux (W m^{-2}) and (b) surface water flux (mm yr^{-1}) into the ocean, (c) SST ($^{\circ}\text{C}$) and (d) SSS, and volume-averaged (e) potential temperature and (f) salinity. Cyan and orange lines show the quantities for the simulations run with the L35 and L20 configurations, respectively.

differences from observations at 5000 m reaching -0.2°C . Differences in salinity from observations, again shown as a global averaged time–depth series, are small (Fig. 2f). Differences of $+0.3$ PSU occur between 300 and 600 m, whilst below 1500 m they are negative and reach a maximum of -0.15 PSU in the abyssal ocean. Differences between L20 and L35 are shown in Fig. 2g and h. L20 exhibits a stronger cooling trend in the deep ocean, such that below 2000 m it is around 0.3°C cooler than L35 after 2000 years. The dipole structure that develops in the time–depth plot of salinity (Fig. 2f) is more pronounced, with the biases at 500 and 3500 m both 25 % stronger in L20 than in L35.

The time series of the maximum AMOC at 30°N is presented in Fig. 3. During the first 300 years of integration, a relatively stable 16–18 Sv is maintained in both the L35 and L20 configurations. After 300 years, both configurations undergo a reduction, with the AMOC in L35 reducing by ~ 4 Sv to 13–15 Sv. The AMOC in L20 reduces initially by ~ 4 Sv and then again around 1250 years into the integration, settling at a value around 10–11 Sv. The weaker AMOC in L20 is consistent with the cooling and freshening trends

seen at depth, since a weaker AMOC allows a greater influence of Antarctic Bottom Water (AABW) in the abyssal ocean. The AMOC values in both simulations are maintained for the remainder of the 2000-year integrations and are within the range of those from the CMIP5 ensemble (Heuzé et al., 2015). The standard deviation of the AMOC based on monthly mean values is 3.5 Sv, which is in reasonable agreement with the magnitude of observed variability (McCarthy et al., 2012). Other than the adjustment in the first 500 years, there is little evidence of emergent decadal or multidecadal variability over the course of the L35 control integration, the peak-to-peak range over the last 1500 years of the integration being 3–4 Sv. The initial strong AMOC followed by a reduction after a few centuries is a common feature of FORTE integrations and appears to be linked to a developing fresh bias over the Greenland, Iceland and Norwegian (GIN) seas (shown later).

Transport through Drake Passage weakens rapidly from an initial value of > 160 Sv, and from the year 200 it settles around 110–115 Sv. This is lower than the recent observation-based estimate of 173 Sv (Donohue et al., 2016)

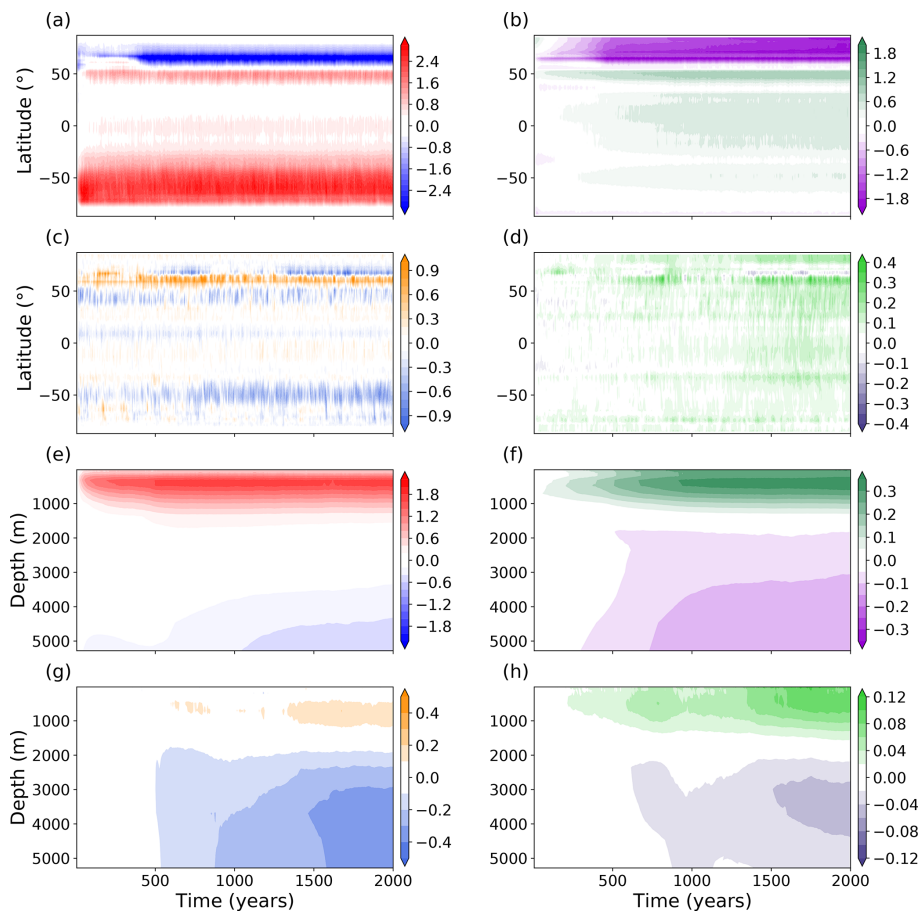


Figure 2. Time–latitude plots of drift in annual mean sea surface (a) temperature ($^{\circ}\text{C}$) and (b) salinity (PSU) in the L35 simulation. Differences (L20–L35) in annual mean sea surface (c) temperature ($^{\circ}\text{C}$) and (d) salinity (PSU). Time–depth series of global drift in annual mean (e) potential temperature ($^{\circ}\text{C}$) and (f) salinity (PSU). Differences (L20–L35) in annual mean (g) potential temperature ($^{\circ}\text{C}$) and (h) salinity (PSU). Drift is relative to initial conditions.

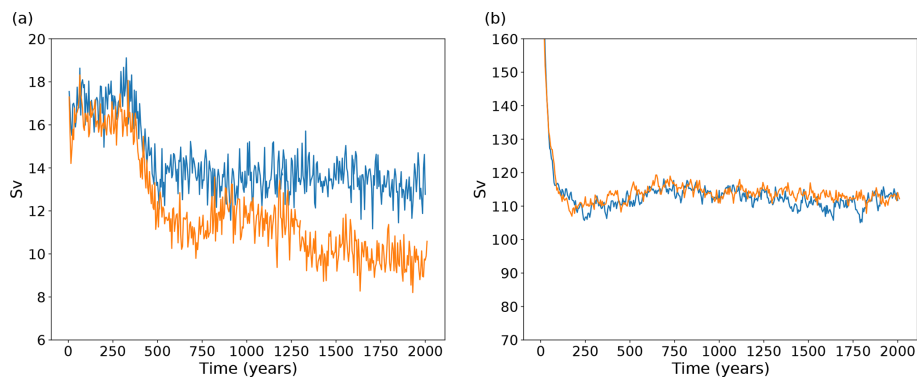


Figure 3. Time series of (a) the 5-year mean AMOC and (b) Drake Passage transport in the control integrations. Cyan (orange) lines show transport for the L35 (L20) configuration.

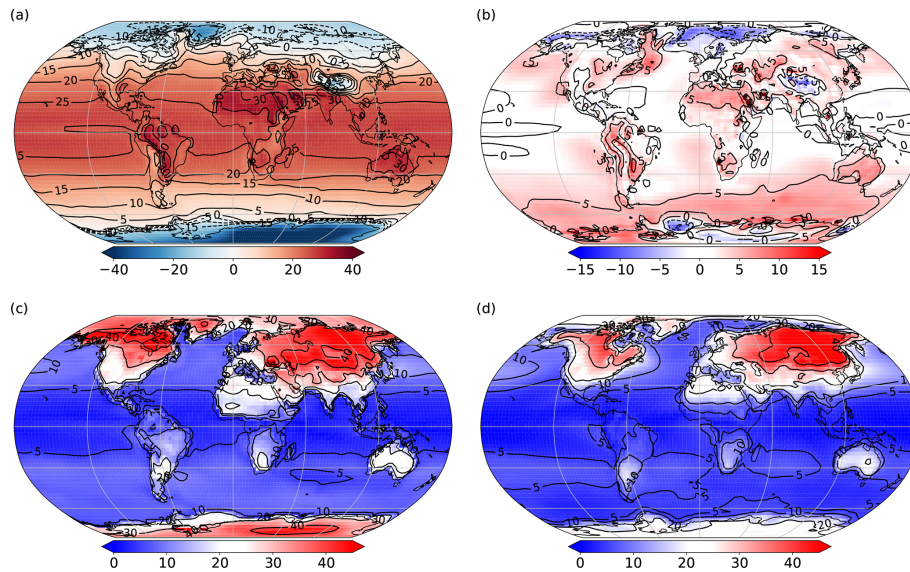


Figure 4. Time mean (years 2001–2025) plots from the L35 configuration showing surface air temperature ($^{\circ}\text{C}$): (a) annual mean, (b) anomaly from 20CR years 1871–1896, (c) seasonal range in FORTE 2.0 and (d) seasonal range in 20CR years 1871–1896.

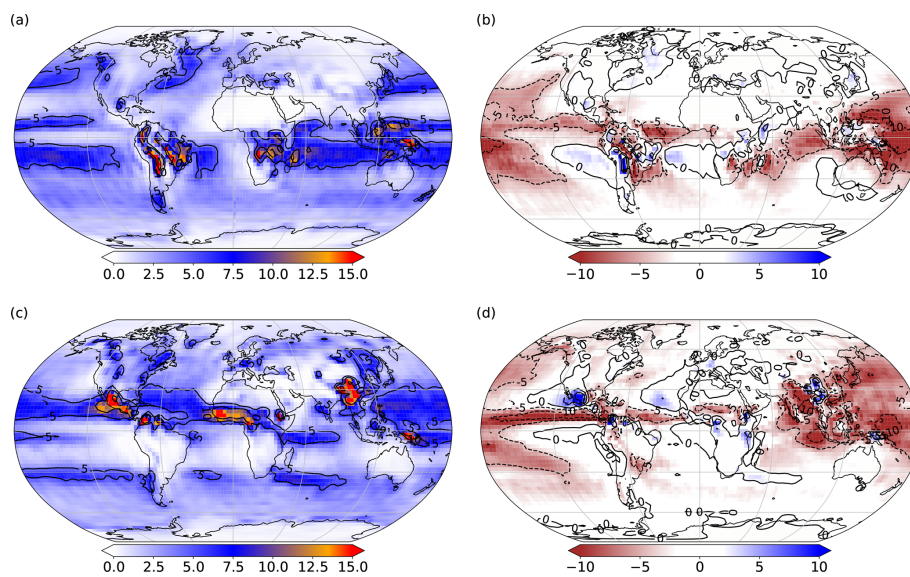


Figure 5. Time mean (years 2001–2025) plots from the L35 configuration showing precipitation (mm d^{-1}): (a) DJF, (b) DJF anomaly from 20CR years 1871–1896, (c) JJA and (d) JJA anomaly from 20CR years 1871–1896.

or previous estimated values of around 130–140 Sv (e.g. Cunningham et al., 2003) but within the range seen in other coupled climate models (Beadling et al., 2020). Kuhlbrodt et al. (2012) show that the strength of the Antarctic Circumpolar Current (ACC) correlates with the choice of GM thickness diffusion, with lower values of κ yielding stronger ACC transport. The L35 and L20 simulations both use a value of $\kappa = 2000$. FORTE 2.0 has a stronger ACC than other models that use $\kappa = 2000$ (see Fig 1b of Kuhlbrodt et al., 2012). It is closer in strength to other models using values of $\kappa = 700$ –1000.

4 The control climate

After the 2000-year spinup, the frequency of output was increased to monthly and a 25-year integration was performed. In this section, the control climate during this 25-year period is presented.

4.1 The atmosphere

Annual time mean surface air temperatures (SATs) in the tropics are 25°C , with some regions over land reaching 30–

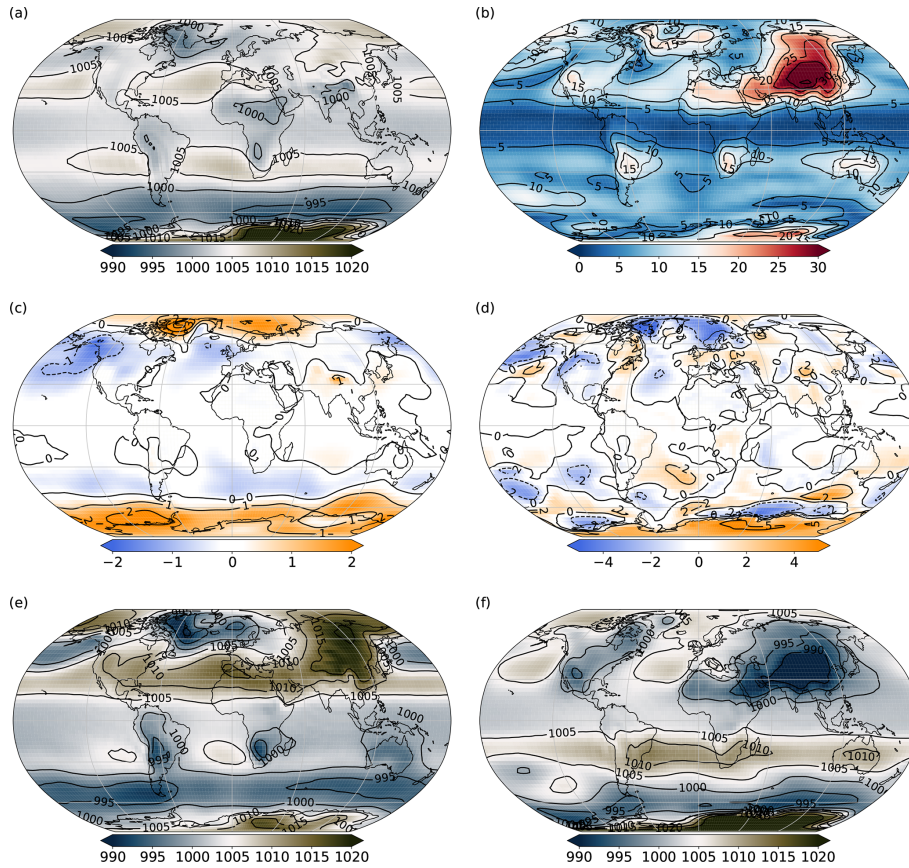


Figure 6. Time mean (years 2001–2025) plots showing sea level pressure (mbar): (a) annual mean, (b) seasonal range, (c) difference in sea level pressure for L20–L35 and (d) difference in seasonal range (L20–L35), plus values for the months of (e) January and (f) July from the L35 simulation.

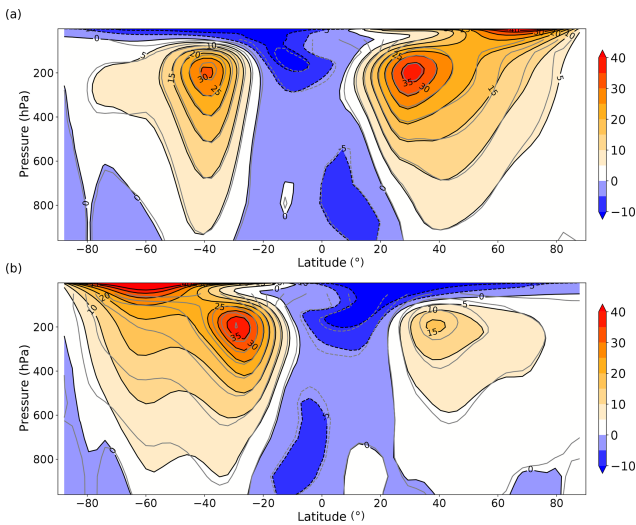


Figure 7. Time and zonal mean zonal wind velocities (m s^{-1}) for (a) winter (DJF) mean and (b) summer (JJA) mean. The shading and black contours show the velocities for the L35 simulation, whilst the grey contours show the equivalent contours for the L20 simulation.

35 °C. The Arctic reaches $-20\text{ }^{\circ}\text{C}$, with temperatures over Greenland reaching as low as $-40\text{ }^{\circ}\text{C}$ and the interior of Antarctica reaches as low as $-60\text{ }^{\circ}\text{C}$ (Fig. 4a). Anomalies of annual mean SAT from the early years (1871–1896) of the 20th Century Reanalysis (20CR; Compo et al., 2011) are presented in Fig. 4b. FORTE 2.0 performs well at low latitudes, especially over the ocean. There is a pronounced warm anomaly of around $5\text{ }^{\circ}\text{C}$ over most of the Southern Ocean, consistent with the positive SST bias shown in Sect. 4.2. A cold SAT anomaly with respect to 20CR also manifests over the Nordic Seas, extending into the Barents Sea. The L20 simulation exhibits very similar annual mean SATs (not shown). Values for L20 are within $1\text{ }^{\circ}\text{C}$ of those shown for the L35, except for two regions over the northern Labrador Sea and the Weddell Sea which are cooler in L20 by several degrees. These differences are likely due to the difference in the response of the flux barrier which represents sea ice. The SAT seasonal ranges for FORTE 2.0 and 20CR (1871–1896) are presented in Fig. 4c and d. Seasonal SAT variability over the tropical ocean is low, whilst variations in SAT over land are much higher, reaching $40\text{ }^{\circ}\text{C}$ over the Eurasian continent. The seasonal range of FORTE 2.0 compares rea-

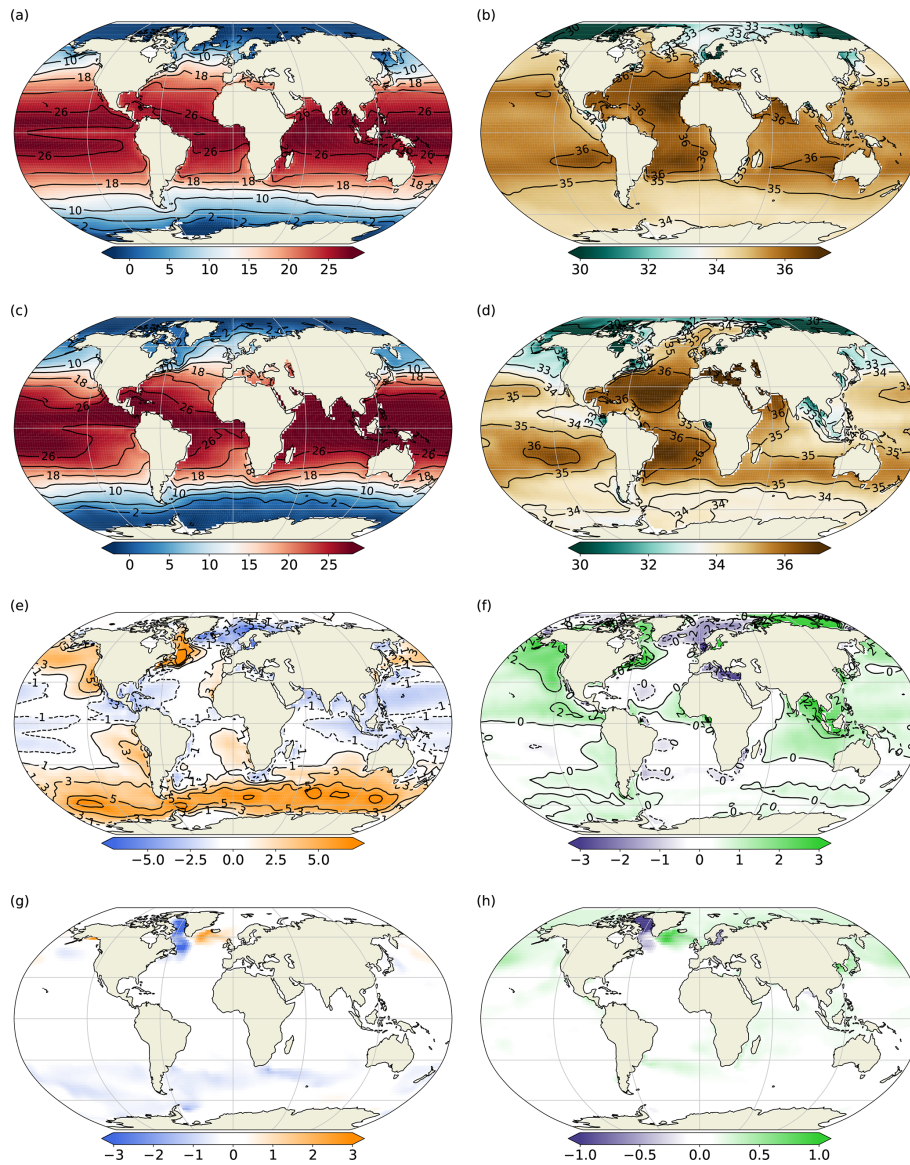


Figure 8. Time mean (years 2001–2025) SST and SSS for FORTE 2.0 L35 (a, b) and for EN3 (c, d). Panels (e) and (f) show FORTE 2.0 L35–EN3 SST and SSS anomalies, respectively, whilst panels (g) and (h) show SST and SSS anomalies for L20–L35.

sonably well with 20CR throughout most of the low and mid-latitudes. However, the seasonal ranges in SAT at high latitudes (both Arctic and Antarctic) are much larger than those in 20CR. Arctic and Antarctic seasonal SAT variability is 40–45 °C, with the coldest regions of Antarctica reaching as low as -85°C during July.

Figure 5 shows winter (DJF) and summer (JJA) mean precipitation and anomalies with respect to the 20CR 1871–1896 climatological mean. During DJF (Fig. 5a), regions of high precipitation over the Northern Hemisphere oceanic western boundary currents (up to 6 mm d^{-1} and extending to northwestern Canada and along the Gulf Stream and western boundary current track in the northwest Atlantic) are evident, as well as high values ($10\text{--}12\text{ mm d}^{-1}$) over trop-

ical Africa and South America, Indonesia and over the Intertropical Convergence Zone (ITCZ) in the Atlantic and Pacific oceans. Very low values ($0\text{--}1\text{ mm d}^{-1}$) are seen over the polar regions, the subtropical desert regions (terrestrial and oceanic) and (unrealistically) over the equatorial Pacific. During summer (JJA), the ITCZ and the corresponding high levels of rainfall shift northward (Fig. 5c). There is enhanced rainfall due to the Asian summer monsoon, though in FORTE 2.0 it does not extend sufficiently far east. The anomalies with respect to the 20CR 1871–1896 climatological DJF mean (Fig. 5b) show that, particularly over the tropical Pacific, FORTE 2.0 simulates too little rainfall. This is most pronounced over the western tropical Pacific during DJF and also over the northern extent of the ITCZ in the east-